ISBN: 978-3-95450-227-1 ISSN: 2673-5490 doi:10.18429/JACoW-IPAC2022-MOPOTK066

DAMPING-RING-FREE INJECTOR DESIGN FOR LINEAR COLLIDERS

T. Xu[1*], M. Kuriki[2], S. Kim[3], P. Piot[1,3], J. G. Power[3],
[1]Northern Illinois University, DeKalb, IL, USA
[2]Hiroshima University, Higashi-hiroshima, Hiroshima, Japan
[3]Argonne National Laboratory, Lemont, IL, USA

Abstract

The current designs of future electron-positron linear colliders incorporate large and complex damping rings to produce asymmetric beams for beamstrahlung mitigation at the interaction point. This paper presents the design of an damping-ring-free electron injector capable of delivering flat electron beams with phase-space partition comparable to the electron-beam parameters produced downstream of the damping ring in the proposed international linear collider (ILC) design. The performance of the proposed configuration, its sensitivity to jitter along with its impact on spin-polarization is discussed.

INTRODUCTION

A technique to mitigate beamstrahlung in linear colliders consists in using flat beams $\sigma_y \ll \sigma_x$ [1]. Flat beams are naturally produced in damping rings (DRs) which generate a beam with asymmetric transverse-emittance partition. It was first recognized in Ref. [2] that a linear transformation exploiting initial cross-plane correlation provides a path to producing flat beams ($\varepsilon_y \ll \varepsilon_x$) in a photoinjector, i.e. without the need for a DR. In Ref. [2] the achievable emittance ratio was comparable to the ones needed for ILC albeit at a much lower (0.5 nC) charge than the required 3.2 nC [3]).

This paper summarized the main results of Ref. [4] where we further expand the technique developed in [2] by combining two cross-plane phase-space manipulations: a round-to-flat beam transformer (RFBT) [2] followed by a transverse-to-longitudinal emittance exchanger (EEX) [5,6]. These phase-space manipulations were developed and experimentally demonstrated over the last two decades [7–11]. It should be noted that a similar approach employing cross-plane phase-space manipulations was proposed in a different parameter range to mitigate the micro-bunching instability in X-ray free-electron lasers (FELs) [6]. Our approach confirms that emittance partition commensurate with requirements for an LC can be attained with a simple and compact (< 50 m) beamline redistributing emittance typically produced in a conventional RF photoinjector.

START-TO-END SIMULATION

The design philosophy focuses on designing an injector capable of minimizing the beam emittance along all d.o.f's upstream of the RFBT, and then optimizing the emittance repartitioning in the RFBT and emittance-exchange process in the EEX beamlines.

* xu@niu.edu

Beam Generation

The conceptual design of the photoinjector beamline from the photocathode surface up to the entrance of the RFBT is diagrammed in Figure 1. The injector beamlines was

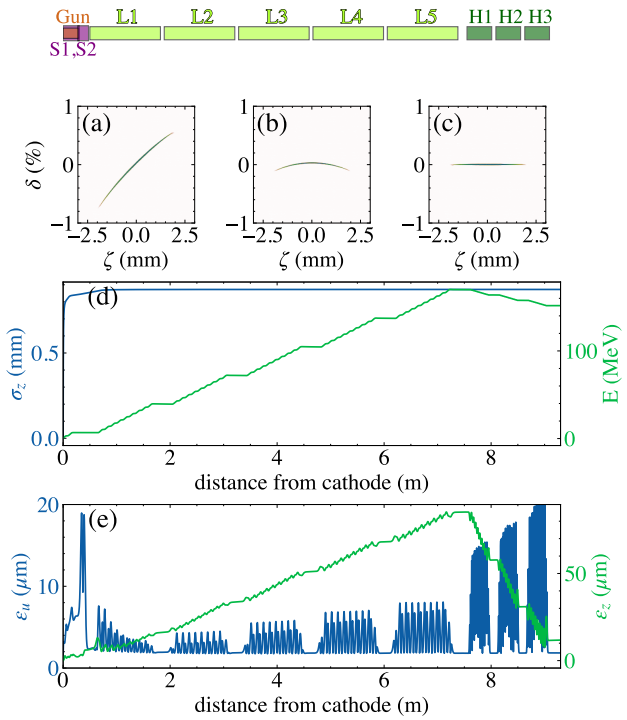

Figure 1: Photoinjector diagram (upper schematics) and snapshots of the LPS distribution at $z = 1.88$ (a), 7.48 (b), and 9.3 m (c) from the photocathode. Evolution of the beam energy and RMS bunch length (d) and corresponding 4D transverse and longitudinal emittances (e). In the upper block diagram, S1 and S2 respectively refer to the solenoidal magnetic lenses, L1-5 are the 1.3-GHz SRF cavities, and H1-3 represent the 3.9-GHz SRF cavities. In plots (a-c) and throughout this paper, $\zeta > 0$ corresponds to the head of the bunch.

modeled using the particle-in-cell beam-dynamics program IMPACT-T [12]. The electron source consists of a $1 + \frac{1}{2}$-cell RF gun operating at $f_0 = 1.3$ GHz operating with a peak field on the cathode of $E_c = 60$ MV/m. The downstream linac consists of five TESLA-type 9-cell superconducting RF (SRF) cavities operating at a peak field of $E_L = 60$ MV/m (corresponding to an accelerating gradient $G_L \simeq E_L/2 \simeq 30$ MV/m consistent with ILC demonstrated requirement of $G_L = 31.5$ MV/m [13]). The RF gun is nested in a pair of solenoidal lenses to control the beam emittance. The

Content from this work may be used under the terms of the CC BY 4.0 licence (© 2022). Any distribution of this work must maintain attribution to the author(s), title of the work, publisher, and DOI

ISBN: 978-3-95450-227-1 ISSN: 2673-5490 doi:10.18429/JACoW-IPAC2022-MOPOTK066

beamline parameters [laser spot radius, solenoid (S1 and S2) strengths and locations, field amplitude and phase of L1] were optimized to minimize the transverse uncorrelated emittance ε_u and maximize the eigenemittance ratio $\varrho \equiv \varepsilon_+/\varepsilon_-$ at the exit of the L1.

To minimize the longitudinal emittance and space-charge effects, we considered a spatiotemporally shaped laser pulse with uniform three-dimensional ellipsoidal intensity distribution [14, 15] which generates linear space charge fields [16, 17]. The linear space-charge force mitigates emittance dilution and imparts a significant chirp in the longitudinal phase space (LPS). Additionally, the resulting bunch length [$\sigma_z \simeq 0.87$ mm; see Fig. 1(a)] leads the LPS to develop a quadratic correlation induced by the RF waveform; see Fig. 1(b). The linac cavities (L2-5) are operated $\varphi_L = 2^\circ$ off-crest to remove the linear LPS correlation after acceleration to 151 MeV; see Fig. 1(b). The 1.3-GHz linacs are followed by a 3rd-harmonic accelerating-cavity module operating at $f_H = 3f_0 = 3.9$ GHz to correct the quadratic correlation in the LPS and reduce the longitudinal emittance. The module comprises three SRF 3rd-harmonic cavities (H1-3) with a similar design as discussed in Ref. [18]. The cancellation of the quadratic correlation gives an 8 fold decrease in the longitudinal emittance to a final value of $\varepsilon_z \simeq 11.78$ μm; see Fig. 1(e). The beamline parameters and resulting beam-emittance partitions are summarized in Table 1.

Table 1: Beamline settings for the proposed photoinjector and achieved normalized-emittance values at the end of the beamline.

parameter	symbol	value	unit
charge	Q	3.2	nC
laser pulse full duration	τ_l	10	ps
laser rms spot size	σ_c	1.93	mm
thermal emittance	ε_c	1.634	μm
magnetic field on cathode	B_c	226	mT
laser/gun launch phase	φ_0[1]	50	deg
peak E field on cathode	E_0	60	MV/m
L2-L5 off-crest phase	φ_L	2	deg
linac peak electric field	E_L	60	MV/m
H1-H3 off-crest phase	φ_H	178.68	deg
H1-H3 peak electric field	E_H	34	MV/m
total beam energy	E_b	151	MeV
longitudinal emittance	ε_z	11.78	μm
transverse eigenemittance	ε_-	6.84	nm
transverse eigenemittance	ε_+	493.4	μm

Emittance Manipulation

The emittance-manipulation beamline comprising the RFBT and EEX sections appears in Figure 2 and was simulated using ELEGANT [19]. The simulations account for higher-order aberrations and bunch self-interaction due to coherent synchrotron radiation (CSR). Downstream of the injector, the magnetized beam is focused by a solenoid into RFBT sections where three skew quadrupoles remove the angular momentum of the magnetized beam and transform the magnetized beam into flat beams with emittance partition downstream of the RFBT $(\varepsilon_{x,f}, \varepsilon_{y,f}, \varepsilon_{z,f}) = (493.40, 7.17 \times 10^{-3}, 11.82)$ μm. This emittance partition confirms that the mapping of the transverse eigenemittances listed in Table 1 to transverse emittance is near ideal (the emittance dilution associated with the mapping $\varepsilon_- \to \varepsilon_y$ is 4.8%) and the longitudinal emittance is preserved (relative emittance growth of 0.3%).

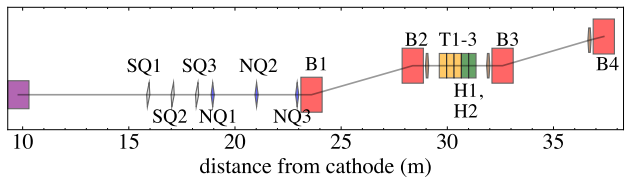

Figure 2: Overview of the emittance manipulation beamline combining the RFBT (skew-quadrupole magnets SQ1, SQ2, and SQ3) and EEX (from dipole magnet B1 to B4) insertions. The label "SQ*i*" and "NQ*i*" refer to skew- and normal-quadrupole magnets, "B*i*" and "E*i*" are dipole nd sextupole magnets. The elements "T*i*" and "H*i*" respectively refer to transverse-deflecting and accelerating SRF cavities; "S3" is a solenoidal magnetic lens.

The flat beam is then matched into the EEX beamlines with NQ1-3 with a certain Courant-Snyder parameters that minimizes emittance growth due to second order effects. The EEX beamline consists of two doglegs each with dipole bending angles of $(+2^\circ, -2^\circ)$, three 3.9-GHz deflecting cavities, and two 3.9-GHz accelerating cavities. The use of multiple SRF cavities is required given the demonstrated cavity performance (maximum achievable deflecting or accelerating voltage) and our requirements. Aside from canceling the thick lens effect of TDC, the accelerating cavities are also used to partially compensate for the correlated energy spread induced by CSR. Additionally, three sextupole magnets (labeled as E1-3) are inserted in the EEX beamline to correct the nonlinearities arising from the deflecting and accelerating 3.9-GHz cavities. The voltages of the TDC and third harmonic cavities, along with the strengths of the sextupole magnet, were numerically optimized to minimize the final horizontal emittance downstream of the EEX beamline. The optimized settings for cavities and magnets appear in Table 2.

The evolution of the beam emittances along the emittance-manipulation section is presented in Fig. 3 and confirms a final emittance partition of $(\varepsilon_{x,e}, \varepsilon_{y,e}, \varepsilon_{z,e}) = (25.47, 7.26 \times 10^{-3}, 546.34)$ μm.

We finally investigated the robustness of the proposed design and the sensitivity of the final transverse emittances to shot-to-shot jitters associated with amplitude and phase stability of the SRF cavities via start-to-end simulations. Specifically, we performed 1000 start-to-end simulations

Content from this work may be used under the terms of the CC BY 4.0 licence (© 2022). Any distribution of this work must maintain attribution to the author(s), title of the work, publisher, and DOI

ISBN: 978-3-95450-227-1 ISSN: 2673-5490 doi:10.18429/JACoW-IPAC2022-MOPOTK066

Content from this work may be used under the terms of the CC BY 4.0 licence (© 2022). Any distribution of this work must maintain attribution to the author(s), title of the work, publisher, and DOI

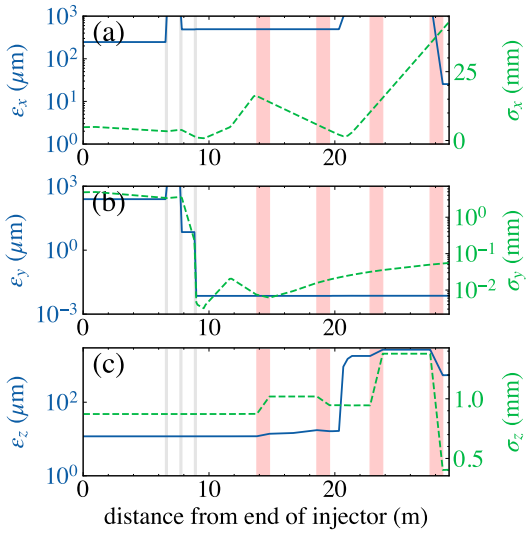

Figure 3: Evolution of the horizontal (a), vertical (b) and longitudinal (c) emittance (blue traces) and bunch size (green dashed traces) along the emittance manipulation beamline (combining the RFBT and EEX transformations). The vertical shaded bands indicate the locations for the RFBT's skew quadrupoles (grey lines at distances < 10 m are for SQ1-3) and dipole magnets (red bands from ~ 14 m to the end of the beamline are for B1-4) associated with the EEX beamline; see Fig. 2.

with different random realizations of the RF amplitude and phase for all the SRF cavities. The amplitude and phase values were randomly generated with a normal distribution with respective rms jitter of 0.01% (fractional deviation from nominal-amplitude settings) and 0.01 degree (for the 1.3 GHz cavities) and 0.03 deg (for the 3.9 GHz cavities). These tolerances are consistent with the performances of the low-level RF system at the European X-ray FEL [20]. These jitter studies confirm that the transverse-emittance fluctuations are acceptable – i.e. $\varepsilon_x = 25.48 \pm 0.02$ µm and $\varepsilon_y = 8.13 \pm 0.98$ nm; see corresponding histogram in Fig. 4.

Table 2: Operating parameters RFBT and EEX beamline, the magnet names refer to Fig. 2.

parameter	value	unit
skew quadrupole magnet SQ1	$k_1 = 3.71$	m^{-1}
skew quadrupole magnet SQ2	$k_1 = -7.08$	m^{-1}
skew quadrupole magnet SQ3	$k_1 = 15.76$	m^{-1}
doglegs dispersion η	-1.67	m
TDC section kick strength κ	6	m^{-1}
dipole magnet B1-B4 angles	2	deg
T1 deflecting voltage	3.72	MV
T2 deflecting voltage	3.72	MV
T3 deflecting voltage	3.66	MV
H4 accelerating voltage	5.81	MV
H5 accelerating voltage	5.91	MV

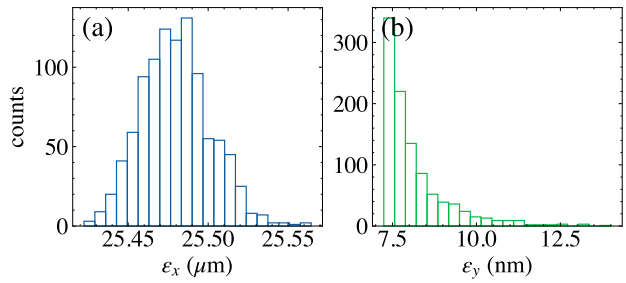

Figure 4: Histogram of final horizontal (a) and vertical (b) emittances simulated downstream of the EEX beamline for 1000 realizations of SRF-cavity random phase and amplitude jitters.

Spin Dynamics

The spin dynamics of the particle distribution was investigated with the beam-dynamics program BMAD [21]. Figure 5 presents the evolution of spin-vector components through the RFBT and EEX sections shown in Fig. 2. The initial conditions are such that the beam is 100% longitudinally spin-polarized $\boldsymbol{S}^T = (0, 0, 1)$. The simulation indicates that the RFBT does not impact the spin (no depolarization is observed) while the EEX beamline yield a small depolarization with final mean and RMS longitudinal spin values being respectively $\langle \boldsymbol{S}_e \rangle^T = (5.41 \times 10^{-5}, -1.39 \times 10^{-8}, 0.99)$ and $(\sigma_{S_{x,e}}, \sigma_{S_{y,en}}, \sigma_{S_{z,e}}) = (1.84 \times 10^{-2}, 1.12 \times 10^{-3}, 1.81 \times 10^{-4})$. confirming that the longitudinal depolarization $\frac{\sigma_{S_{z,e}}}{\langle S_{z,e} \rangle} \sim O(10^{-4})$ is insignificant .

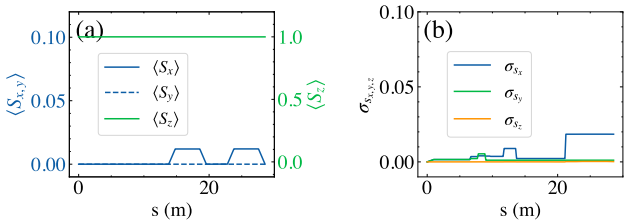

Figure 5: Evolution of the spin components along the emittance-manipulation beamline. Spin components $\mathbf{S}^T = (S_x, S_y, Sz)$ statistical average $\langle \mathbf{S} \rangle$ (a) and RMS value $\langle \mathbf{S}^2 \rangle^{1/2}$ (b) computed over the macroparticle distribution.

CONCLUSION

In summary, we demonstrated a beamline composed of two cascaded cross-plane manipulations that could produce an electron beam with a final transverse-emittance partition comparable to the one attained downstream of the damping ring in the ILC design. The proposed scheme presents a substantial cost and complexity reduction compared to a damping ring. Although our focused was on demonstrating the application of the scheme to ILC-like parameters, the concept also be optimized for other LC designs.

ISBN: 978-3-95450-227-1 ISSN: 2673-5490 doi:10.18429/JACoW-IPAC2022-MOPOTK066

REFERENCES

[1] K. Yokoya, "Beam-beam interaction in linear collider," *AIP Conference Proceedings*, vol. 592, no. 1, pp. 185–204, 2001.

[2] R. Brinkmann, Y. Derbenev, and K. Flöttmann, "A low emittance, flat-beam electron source for linear colliders," *Phys. Rev. ST Accel. Beams*, vol. 4, p. 053501, May 2001.

[3] N. Phinney, N. Toge, and N. Walker, "ILC reference design report volume 3 - accelerator," 2007.

[4] T. Xu, M. Kuriki, P. Piot, and J. Power, "Proposal for a damping-ring-free electron injector for future linear colliders," *ArXiV:2205.03736*, 2022.

[5] M. Cornacchia and P. Emma, "Transverse to longitudinal emittance exchange," *Phys. Rev. ST Accel. Beams*, vol. 5, p. 084001, Aug 2002.

[6] P. Emma, Z. Huang, K.-J. Kim, and P. Piot, "Transverse-to-longitudinal emittance exchange to improve performance of high-gain free-electron lasers," *Phys. Rev. ST Accel. Beams*, vol. 9, p. 100702, Oct 2006.

[7] P. Piot, Y.-E. Sun, and K.-J. Kim, "Photoinjector generation of a flat electron beam with transverse emittance ratio of 100," *Phys. Rev. ST Accel. Beams*, vol. 9, p. 031001, Mar 2006.

[8] J. Ruan, A. S. Johnson, A. H. Lumpkin, R. Thurman-Keup, H. Edwards, R. P. Fliller, T. W. Koeth, and Y.-E. Sun, "First observation of the exchange of transverse and longitudinal emittances," *Phys. Rev. Lett.*, vol. 106, p. 244801, Jun 2011.

[9] Y.-E. Sun, P. Piot, A. Johnson, A. H. Lumpkin, T. J. Maxwell, J. Ruan, and R. Thurman-Keup, "Tunable subpicosecond electron-bunch-train generation using a transverse-to-longitudinal phase-space exchange technique," *Phys. Rev. Lett.*, vol. 105, p. 234801, Dec 2010.

[10] L. Groening, M. Maier, C. Xiao, L. Dahl, P. Gerhard, O. K. Kester, S. Mickat, H. Vormann, M. Vossberg, and M. Chung, "Experimental proof of adjustable single-knob ion beam emittance partitioning," *Phys. Rev. Lett.*, vol. 113, p. 264802, Dec 2014.

[11] G. Ha, M. Cho, W. Gai, K.-J. Kim, W. Namkung, and J. Power, "Perturbation-minimized triangular bunch for high-transformer ratio using a double dogleg emittance exchange beam line," *Phys. Rev. Accel. Beams*, vol. 19, no. 12, p. 121301, 2016.

[12] J. Qiang, S. Lidia, R. D. Ryne, and C. Limborg-Deprey, "Three-dimensional quasistatic model for high brightness beam dynamics simulation," *Phys. Rev. ST Accel. Beams*, vol. 9, p. 044204, Apr 2006.

[13] D. Broemmelsiek, B. Chase, D. Edstrom, E. Harms, J. Leibfritz, S. Nagaitsev, Y. Pischalnikov, A. Romanov, J. Ruan, W. Schappert, V. Shiltsev, R. Thurman-Keup, and A. Valishev, "Record high-gradient SRF beam acceleration at fermilab," *New Journal of Physics*, vol. 20, p. 113018, nov 2018.

[14] Y. Li and J. W. Lewellen, "Generating a quasiellipsoidal electron beam by 3D laser-pulse shaping," *Phys. Rev. Lett.*, vol. 100, p. 074801, Feb 2008.

[15] Y. Li, S. Chemerisov, and J. Lewellen, "Laser pulse shaping for generating uniform three-dimensional ellipsoidal electron beams," *Phys. Rev. ST Accel. Beams*, vol. 12, p. 020702, Feb 2009.

[16] P. M. Lapostolle, "Effets de la charge d'espace dans un accélérateur linéaire à protons," Tech. Rep. CERN-AR-Int-SG-65-15, CERN, Geneva, Jul 1965.

[17] O. J. Luiten, S. B. van der Geer, M. J. de Loos, F. B. Kiewiet, and M. J. van der Wiel, "How to realize uniform three-dimensional ellipsoidal electron bunches," *Phys. Rev. Lett.*, vol. 93, p. 094802, Aug 2004.

[18] M. Bertucci, A. Bignami, A. Bosotti, P. Michelato, L. Monaco, C. Pagani, R. Paparella, D. Sertore, C. Maiano, P. Pierini, and J. Chen, "Performance analysis of the European X-ray Free Electron Laser 3.9 GHz superconducting cavities," *Phys. Rev. Accel. Beams*, vol. 22, p. 082002, Aug 2019.

[19] M. Borland, "ELEGANT: A Flexible SDDS-Compliant Code for Accelerator Simulation," in *6th International Computational Accelerator Physics Conference (ICAP 2000)*, 2000.

[20] M. Omet *et al.*, "LLRF Operation and Performance at the European XFEL," in *Proc. IPAC'18*, pp. 1934–1936, JACoW Publishing, Geneva, Switzerland. doi:10.18429/JACoW-IPAC2018-WEPAF051.

[21] D. Sagan, "Bmad: A relativistic charged particle simulation library," *Nuclear Instruments and Methods in Physics Research Section A: Accelerators, Spectrometers, Detectors and Associated Equipment*, vol. 558, pp. 356–359, Mar. 2006.

Content from this work may be used under the terms of the CC BY 4.0 licence (© 2022). Any distribution of this work must maintain attribution to the author(s), title of the work, publisher, and DOI